




# Effect of Al addition and rolling reduction on microstructure and texture evolution of Mg–3Sn alloy during high-speed rolling

Di Pei<sup>1</sup>, Li Wang<sup>2</sup>, Xuhao Hu<sup>1</sup>, Xinlin Li<sup>1,\*</sup> , and Xiang Wang<sup>1</sup>

<sup>1</sup> Key Laboratory of Superlight Materials and Surface Technology, Ministry of Education, College of Materials Science and Chemical Engineering, Harbin Engineering University, 145 Nantong St., Harbin 150001, People's Republic of China

<sup>2</sup> Chongqing Gearbox Co., Ltd., Chongqing 401122, People's Republic of China

**Received:** 1 August 2023

**Accepted:** 25 September 2023

**Published online:**  
9 October 2023

© The Author(s), under exclusive licence to Springer Science+Business Media, LLC, part of Springer Nature, 2023

## ABSTRACT

In this study, high-speed rolling is conducted on Mg– $x$ Al–3Sn ( $x = 0, 3, 6$ ) alloys with different reductions (20%, 40%, 60%, and 70%), at a high speed of 1100 m/min and a high temperature of 400 °C. This process imposes a considerable reduction in a single pass. Results indicate that twinning is the primary deformation mechanism, and the prominent nucleation mechanism is twinning-induced continuous dynamic recrystallization (CDRX). In the initial stage, numerous twins with high dislocation density and low angle grain boundaries (LAGBs) are generated. Then, due to the insufficient time for the transformation from LAGBs to high angle grain boundaries (HAGBs), substructures and subgrains are formed within twins as the potential nuclei for recrystallized grains. Furthermore, the orientation of substructures formed by twinning-induced CDRX is decided by the initial twin style. Texture evolution reveals that DRX behavior is the main factor influencing the basal texture. ATZ331 samples exhibit the lowest maximum basal texture intensity irrespective of the rolling reductions. When the rolling reduction ranges from 20 to 60%, the maximum texture intensity of all these three alloys first decreases and then increases. However, with the further increase in the rolling reduction to 70%, the basal texture of Mg–3Sn and ATZ631 samples weakens, while that of the ATZ331 sample enhances.

## Introduction

Magnesium (Mg) sheets have attracted significant research attention, owing to their low density, high specific strength, and specific stiffness [1]. However,

hexagonal close-packed (HCP) structure, strong basal texture and a limited number of slip systems lead to poor formability, which hinders their application prospects [2].

Handling Editor: Naiqin Zhao.

Address correspondence to E-mail: [lixinlin@hrbeu.edu.cn](mailto:lixinlin@hrbeu.edu.cn)

<https://doi.org/10.1007/s10853-023-08990-7>

Recently, high-speed rolling (HSR, the rolling speed  $> 200$  m/min) has been reported as an effective method to weaken the basal texture and improve the formability [3]. On one hand, the basal texture can be weakened by HSR, which activates non-basal slip and twins. Su [4] reported that many twins and  $\langle c+a \rangle$  slip could be activated in AZ31 alloy at the rolling speed of 1000 m/min and temperature of 100 °C because the temperature during HSR could be increased to 482 °C at the rolling reduction of 72% in a single pass. On the other hand, dynamic recrystallization (DRX) can be promoted during HSR. Kim [5] reported that fully recrystallized grains of AZ31 alloy were obtained at a large reduction in a single pass at the rolling speed of 470 m/min and temperature of 400 °C. Twinning-induced DRX exhibits priority over the bulging of grain boundaries (GBs) due to the insufficient time during HSR. Notably, HSR can suppress dislocation slips but promote twinning. In general, DRXed grains exhibit an off-basal orientation, and the distribution of the DRXed this region is broader than that of unDRXed region during HSR, thereby weakening the basal texture [6]. The basal texture intensity of DRXed regions can be weakened in AZ31 during HSR because  $c$ -axes of new grains are widely spread along normal direction (ND). However, previous literatures about Mg alloys subjected to HSR mainly focused on the AZ31 alloy.

In the past decade, Mg–Sn-based alloys have attracted extensive research. Compared with other alloying elements, Sn addition can weaken the basal texture by activating non-basal slip systems because of the decrease in the critical resolved shear stress (CRSS) of  $\langle c+a \rangle$  slip systems [7, 8]. The generalized stacking fault energy can also be reduced in the prismatic  $\{10\text{--}11\} \langle 11\text{--}20 \rangle$  and  $\{11\text{--}22\} \langle 11\text{--}23 \rangle$  slip systems with the addition of Sn [9]. In general, aluminum (Al) element is also an important alloying element to weaken the texture. However, the effect of Al addition on DRX is controversial. According to some literature studies,  $\text{Mg}_{17}\text{Al}_{12}$  phase can easily precipitate during plastic deformation and promote DRX by particle stimulated nucleation mechanism [10]. Higher content of Al addition can lead to the rotation of the  $c$ -axes of grains against the compression direction in AZ91 alloy [11]. Conversely, Al addition can inhibit twinning nucleation and GB migration in Mg–Al alloys, thereby inhibiting twinning-induced DRX [12]. However, systemic study on DRX behavior and macrotexture evolution with the

addition of Al during HSR has never been reported to date.

In our previous research, only the microstructure and microtexture evolution of twin bands region of Mg– $x$ Al–3Sn ( $x = 0, 3, 6$ ) samples was studied with the rolling reduction of 40% [13]. In this study, systematic investigation was carried out to evaluate the effect of Al addition and rolling reduction (20–70%) on DRX behavior and macrotexture evolution of as-homogeneous Mg– $x$ Al–3Sn ( $x = 0, 3, 6$ ) alloys at a high temperature of 400 °C and a high speed of 1100 m/min.

## Experimental

As-homogenized Mg– $x$ Al–3Sn alloys were machined to an initial size of 100 mm (RD)  $\times$  60 mm (TD)  $\times$  2 mm (ND). Then, the samples were rolled with a twin-roll with various rolling reduction (20%, 40%, 60% and 70%) at a rolling speed of 1100 m/min and a temperature of 400 °C.

X-ray diffraction (XRD) analysis was used to analyze the crystal phases and macrotexture of the samples with Cu  $K\alpha$  radiation at an operating voltage of 40 kV and an operating current of 150 mA, which were measured along the RD–TD. Optical microscopy (OM) was used to observe the microstructural on RD–ND. Transmission electron microscopy (TEM) was used to observe microstructure evolution on RD–TD. Recrystallized volume frequency, twin style, and misorientation distribution were examined by electron backscatter diffraction (EBSD). The accelerating voltage was 20 kV, and the scan steps were 0.3  $\mu\text{m}$  on RD–ND. Data were processed by using Channel 5.0.

## Results and discussion

### Precipitation behavior

Figure 1 exhibits the XRD pattern, confirming the presence of  $\alpha$ -Mg phase and  $\text{Mg}_2\text{Sn}$  phase are detected, as shown in Fig. 1. Results show that Al addition can inhibit the  $\text{Mg}_2\text{Sn}$  precipitation, because Al atoms dissolved in the matrix serve as a diffusion barrier to the Sn atoms [14]. Furthermore, BSE-SEM images of the samples with the rolling reduction of 70% are shown in Fig. 2. Results show that the number of  $\text{Mg}_2\text{Sn}$  precipitates decreases dramatically with increasing Al content. Furthermore, a few second phases get

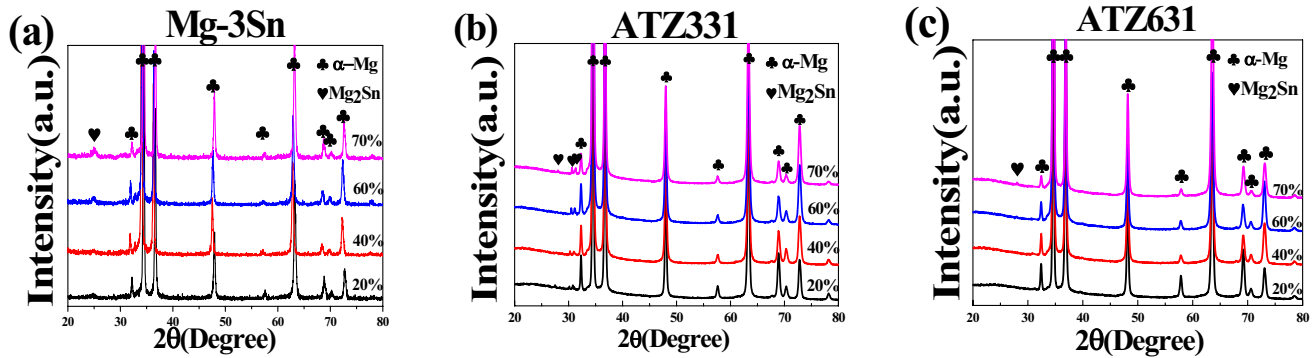


**Figure 1** XRD patterns of the HSRed Mg- $x$ Al-3Sn alloys with different rolling reductions.

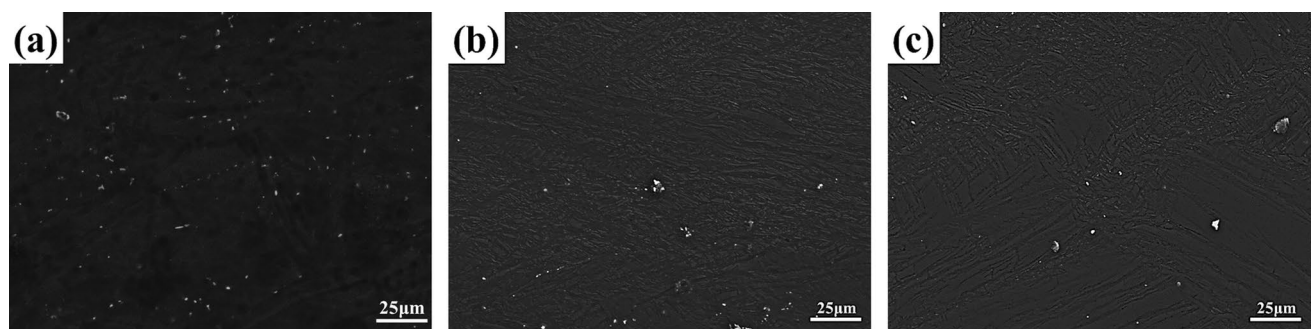


**Figure 2** BSE-SEM images of the samples with the rolling reduction of 70%: **a** Mg-3Sn, **b** ATZ331, and **c** ATZ631.

precipitated during HSR. This is attributed to the fact that the combined action of HSR, high rolling temperature and high temperature-rise during HSR, results in an increased solid solubility. Thus, the effect of the second phase during HSR can be negligible.

### Microstructure evolution

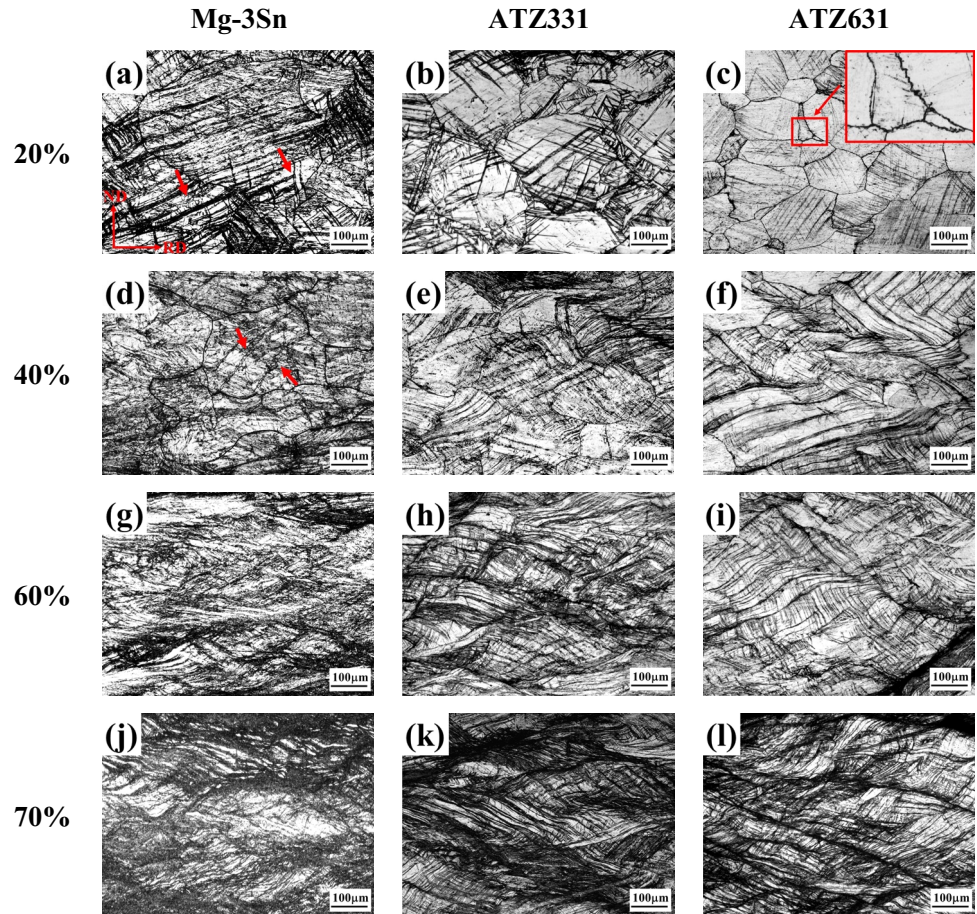
Figure 3 shows OM images of the HSRed Mg- $x$ Al-3Sn alloys with different rolling reductions. Clearly, numerous deformation twins are activated, which break the original grains into smaller pieces. Therefore, twinning is the primary deformation mechanism because the slip systems are not available to be triggered simultaneously [15]. Thus, GB slipping unlikely plays a significant role in this process. For the Mg- $x$ Al-3Sn samples with the rolling reduction of 20%, numerous twins are easily formed. However, with the increase in the Al content, the frequency of twins decreases. It shows that Mg alloys with lower Al content exhibit a reduced tendency to develop serrated GBs, revealing Al addition can inhibit twinning. This is because the CRSS of twinning nucleation increases with the added content of Al element [16]. Moreover,

as shown by arrow in Fig. 3c, the GBs are serrated into the bulge due to stress generated from the substructures and regional differences in dislocation density [17]. This can be frequently observed as a prelude to discontinuous dynamic recrystallization (DDR<sub>X</sub>) [18], and the GBs move from the high dislocation density side to the low dislocation density side. Furthermore, with the increase in the rolling reduction from 20 to 70%, the deformed grains are elongated along the RD, and the twins become fine and homogeneous.

### Dynamic recrystallization behavior

First, inverse pole figure (IPF) maps of the HSRed Mg- $x$ Al-3Sn-20% samples are shown in Fig. 4a, d, g. Results show the presence of numerous LAGBs in all the samples, marked by the gray lines. This is attributed to the fact that the original coarse grains undergo significant deformation, and the accumulated strain cannot be released during HSR. Furthermore, Kernel average misorientation (KAM) maps show that the DRXed regions possess the lowest strain, while GBs and twinning regions possess high strain. Other sky-blue regions (marked by the white arrows) within

**Figure 3** OM of the HSRed Mg-*x*Al-3Sn alloys with various rolling reductions.



initial coarse grains possess lower strain, revealing that Al addition can decrease the average value of KAM, because twins decrease with the addition of Al element, which typically have higher strain during HSR [19]. Figure 4c, f, i shows that a small amount of DRXed grains can be found at the GBs and twins, revealing the nucleation of DRXed grains caused by bulging of GBs or twin boundaries (TBs). Moreover, substructures are the primary microstructure, revealing that the misorientation within the unDRXed regions easily exceeds  $2^\circ$  during HSR. In order to verify this conclusion, different types of grains of Mg-*x*Al-3Sn samples with the rolling reduction of 40% and 60% are investigated, as presented in Fig. 5. Further, different types of grains of Mg-*x*Al-3Sn alloys with the rolling reduction of 20%, 40% and 60% are shown in Fig. 6. Results reveal that the main microstructure is substructure of all the samples investigated in this study, which can serve as the potential nuclei for recrystallization [20]. The frequency of substructure in Mg-*x*Al-3Sn samples decreases with the increase in the Al content from 3 to 6 wt% regardless of

the rolling reduction. Therefore, low Al levels promote DRX, while high Al levels inhibit DRX. Notably, the ATZ331 alloys with various rolling reductions exhibit the highest frequency of substructures, in particular, the ATZ331-40% sample.

ATZ331-60% sample is examined by TEM to reveal more microstructural features related to DRX behavior, as shown in Fig. 7. Clearly, twinning is dominant plastic deformation mechanism, and a large proportion of grains is still unDRXed. Moreover, twins acquire the bamboo-shaped structure, and the potential nuclei for recrystallization are formed within twins, marked by the red arrows in Fig. 7a. Figure 7b shows that twins induced by HSR are filled with high density of dislocation lines and LAGBs, marked by the yellow and the red arrows, respectively. Furthermore, substructures are formed by the interaction between dislocations and LAGBs, which can serve as the potential nuclei for recrystallization, as shown in Fig. 7d. Then, the formation of subgrains occurs within the twin. The initial TB undergoes deformation and the sub-GB bulges, as

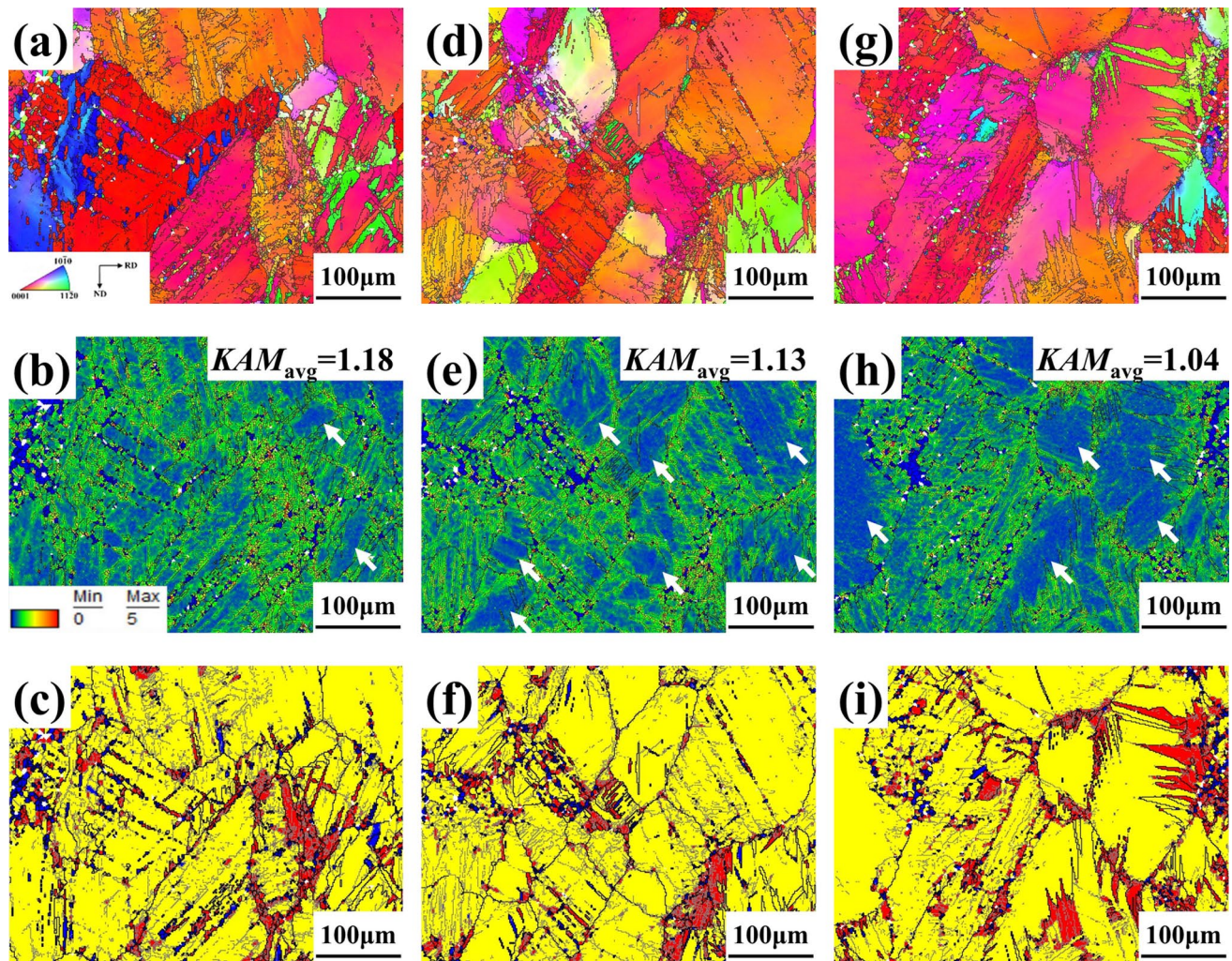


**Figure 4** IPF maps, KAM maps and different types of grains (blue-recrystallized grains, yellow-substructures, red-deformed grains) of the samples with the rolling reduction of 20%: **a–c** Mg–3Sn, **d–f** ATZ331, and **g–i** ATZ631 alloy.

shown in Fig. 7e. Finally, the initial coarse grains are consumed during this process by the formation of subgrains and DRXed grains via CDRX, marked by the yellow and the red arrows in Fig. 7f. It indicates that the nucleation mechanism during this process is twinning-induced CDRX.

The microstructures of Mg– $x$ Al–3Sn alloys with the rolling reduction of 60% at high magnification are shown in Fig. 8. The initial grains appear to be separated by a significant number of twins. In Mg–3Sn alloy, parts of initial matrix microstructure still remain, and fine recrystallized grains are observed in the local twinning areas, as marked by the red lines in Fig. 8a. However, in ATZ331 alloy and ATZ631 alloy, numerous twins including parallel twins, intersecting twins and secondary twins are formed, resulting

in fine grains. However, the highest proportion of unDRXed regions remain in ATZ631 alloy.

Then, EBSD maps of the samples with 60% rolling reduction are shown in Fig. 9. IPF maps show that large numbers of LAGBs are extensively present in grains, as indicated by the gray lines. It shows that the strain energy is still stored as defects in the large grain. IPF maps show the generation of complex microstructures, which include numerous banded structures separated by LAGBs, deformed grains, and DRXed grains. Evidently, new fine grains mainly develop from twin areas. High strain energy gets easily accumulated in twins, resulting in the formation of substructures within twins [21, 22]. The presence of twins created a zone with a significant orientation gradient that is the perfect location for recrystallization [23]. This result

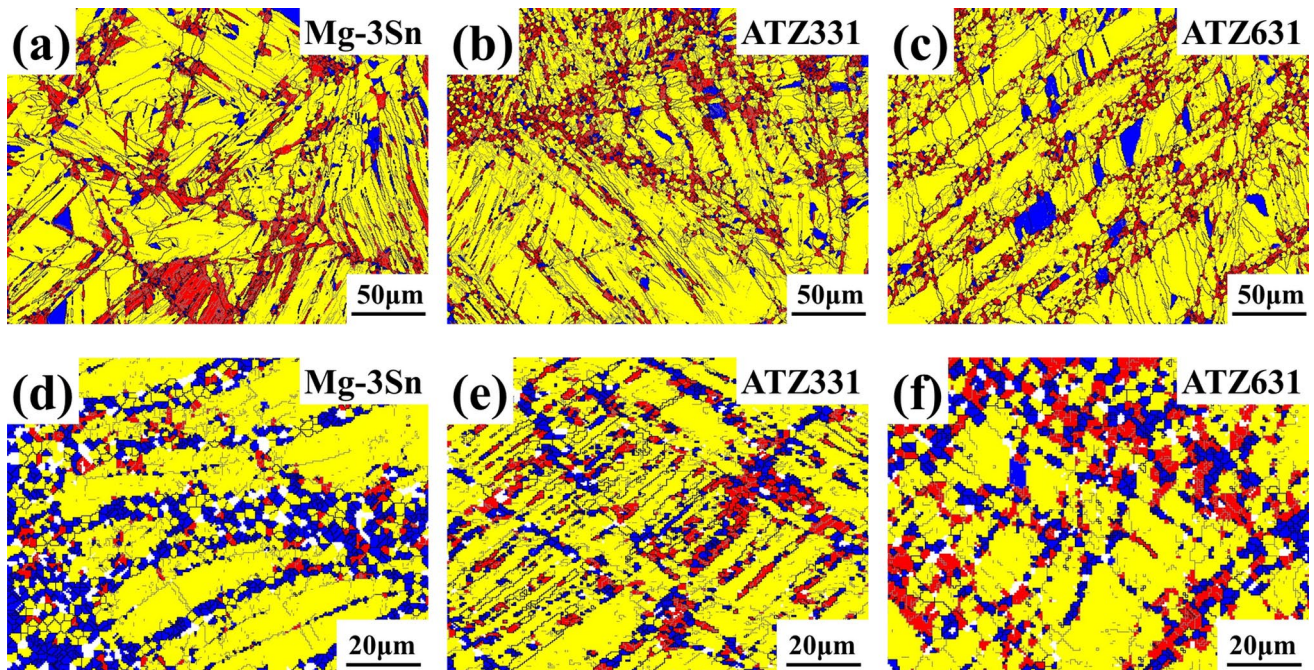


**Figure 5** Different types of grains of the Mg- $x$ Al-3Sn samples with the rolling reductions of **a–c** 40% and **d–f** 60%: blue-recrystallized grains, yellow-substructures, red-deformed grains.

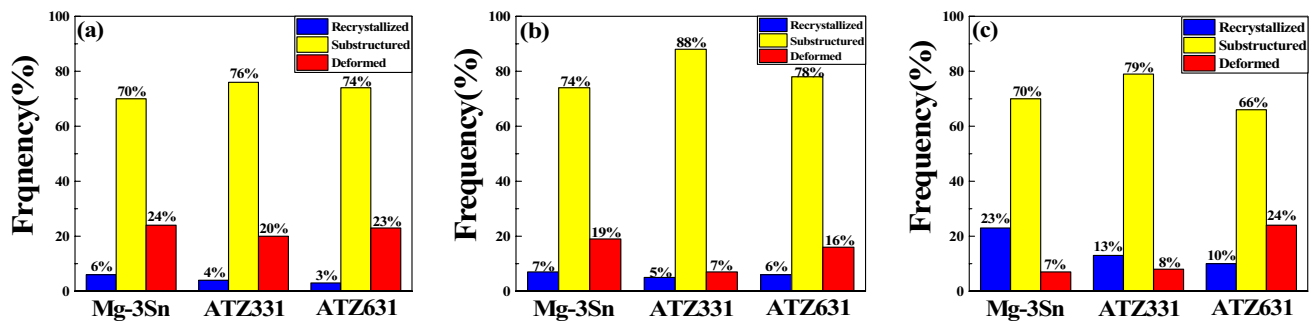
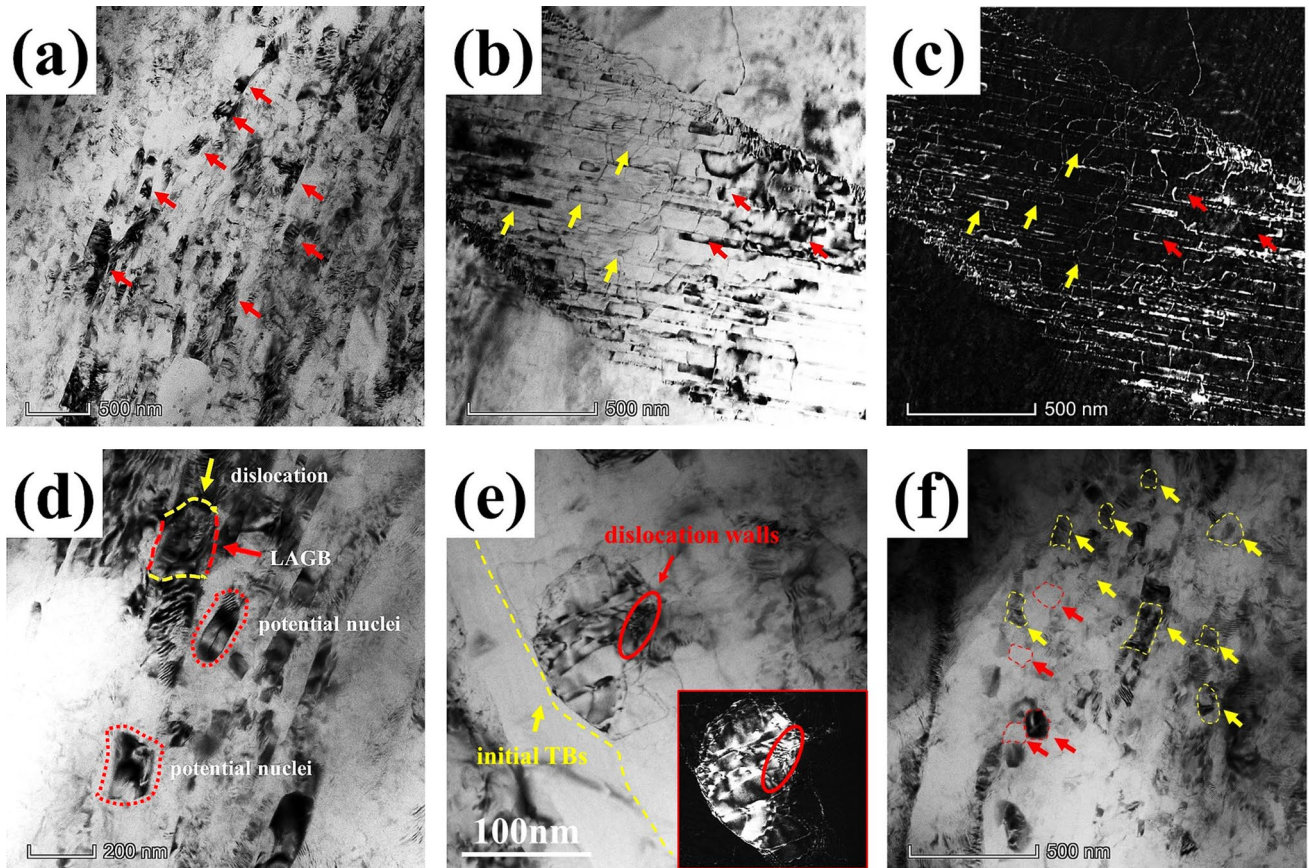


**Figure 6** The frequency of the samples with the rolling reduction of **a** 20%, **b** 40%, and **c** 60%.

shows that the nucleation mechanism is dominated by twinning-induced DRX. In general, DDRX mechanism is dominant at the temperature of 400 °C, and however, there is insufficient time for bulging of GBs during HSR. Therefore, twinning-induced CDRX is the dominant nucleation mechanism. Moreover, Fig. 9d–f shows that the strain in the DRXed regions is significantly lower compared to that in other areas. Owing to the consumption of strain energy stored in the DRXed regions, it exhibits a lower KAM value. ATZ331-60% sample possesses the highest average value of KAM. Thus, it can be inferred that the HSRed ATZ331 alloy can more quickly obtain the microstructure with fully

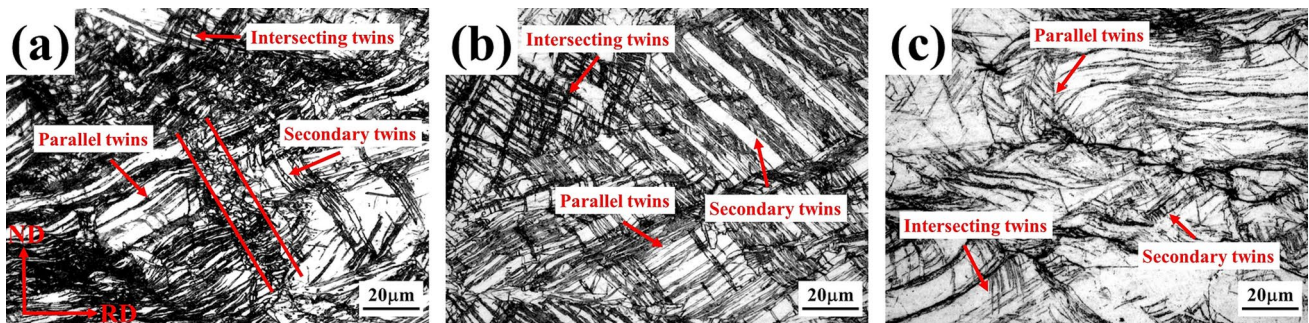
recrystallized grains than Mg-3Sn and ATZ631 alloys during subsequent annealing process.

Figure 10 shows a selected region of Fig. 9b including substructures formed within twins of the ATZ331-60% sample, and the average misorientation angles of grains are investigated. The misorientation angles of these substructures are 35.1° ~ 42.7°, which are caused by lattice reorientation within twins, and are significantly related to the 38° {10-11}–{10-12} double twins (DTs) [24]. Moreover, many LAGBs are also present within twin regions. Results show that in this process, the formation of substructures occurs through twinning-induced CDRX. The orientation of the



**Figure 7** TEM microstructures of the ATZ331-60% sample. **a** Twinning-induced DRX nucleation mechanism; **b** bright field image of high dislocation density within twins; **c** dark field image of high dislocation density within twins; **d** CDRX nuclea-

tion within twins; **e** the formation of subgrains within twins; **f** subgrains and DRXed grains, marked by yellow arrows and red arrows.



**Figure 8** OM of the microstructure of the samples with the rolling reduction of 60% at high magnification: **a** Mg-3Sn, **b** ATZ331, and **c** ATZ631 alloy.

substructures formed is primarily influenced by the initial twins.

For systematic analysis of the effect of twins on microstructural evolution, the types and the proportion of twins in Mg-*x*Al-3Sn samples with the rolling

reduction of 20% and 60% are examined, as shown in Fig. 11, and the results are shown in Fig. 12. Figure 11 exhibits that the twinning types are 38° {10-11}–{10-12} DTs, 56° {10-11} contraction twins (CTs) and 86° {10-12} extension twins (ETs). When the rolling reduction

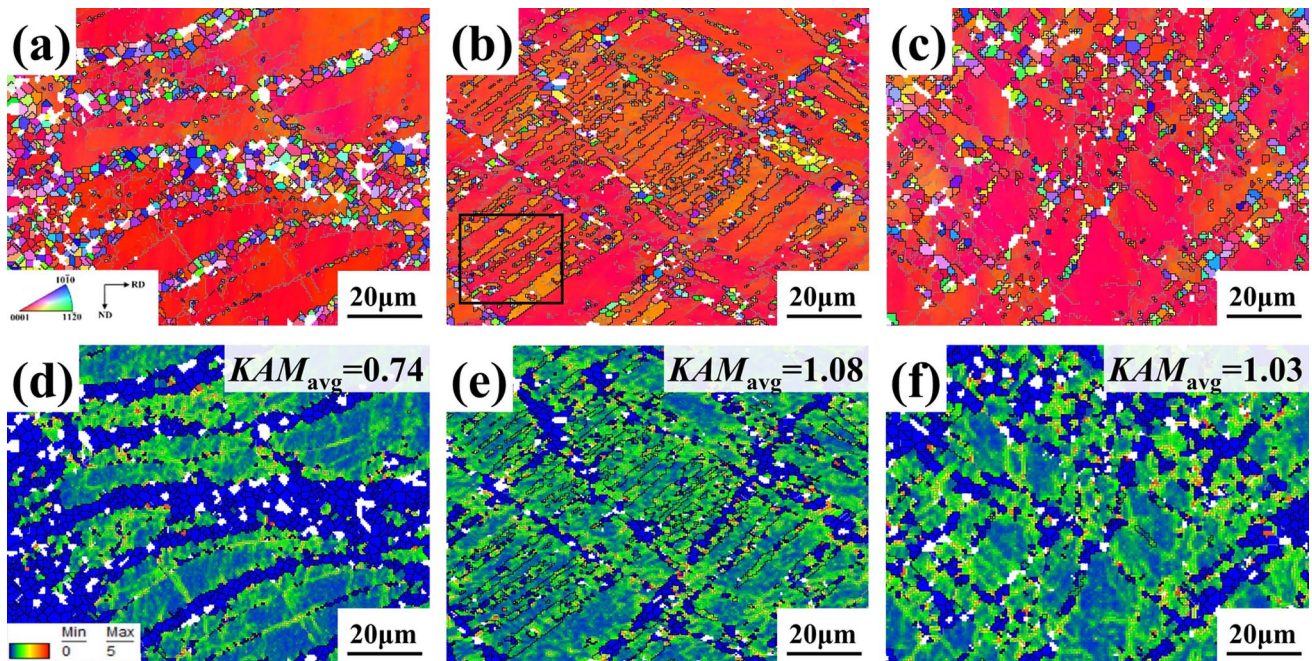


**Figure 9** IPF maps, different types of grains and KAM maps of the samples with the rolling reduction of 60%: **a, d** Mg–3Sn, **b, e** ATZ331, and **c, f** ATZ631 alloy.

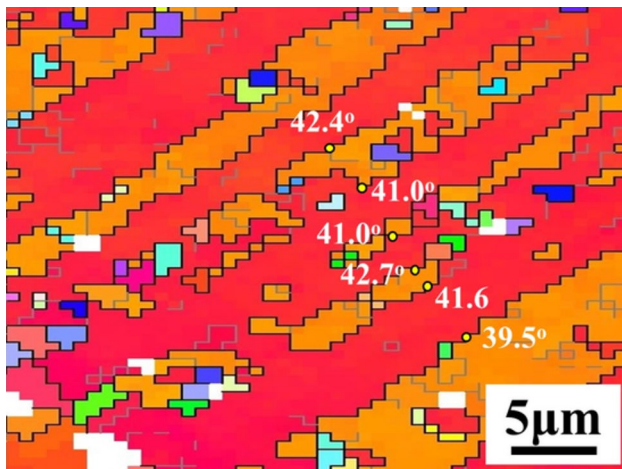


**Figure 10** IPF maps showing the selected region of Fig. 9b.

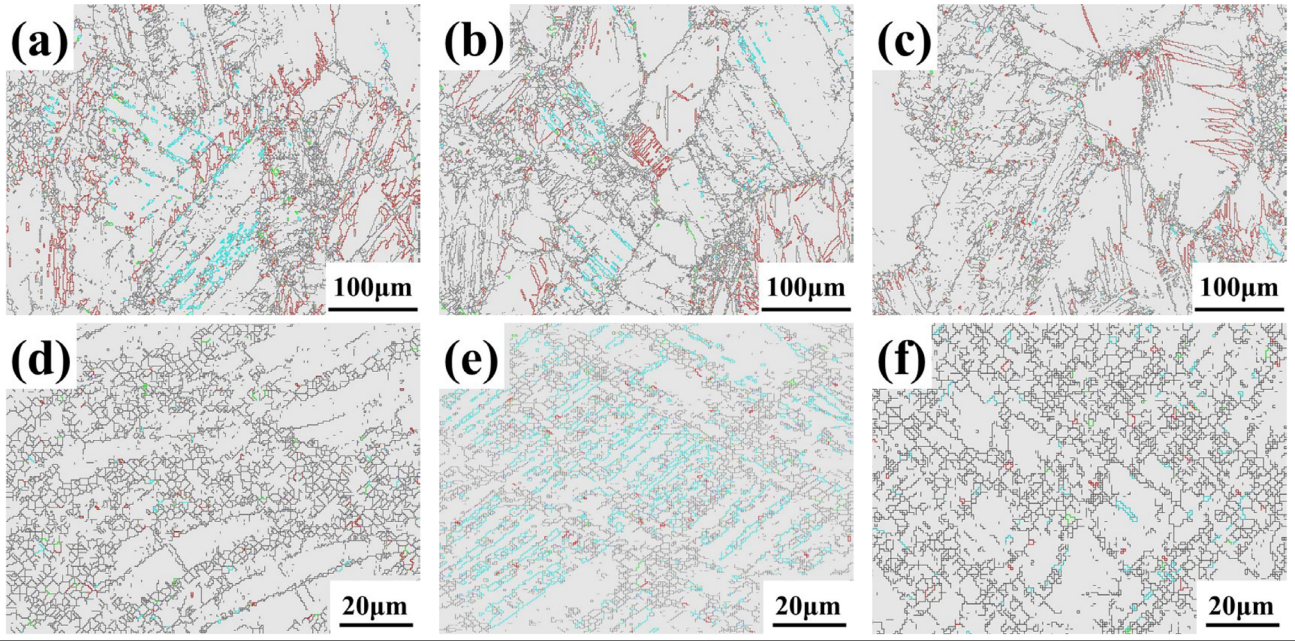
is smaller, the proportion of ETs is the highest, followed by DTs and CTs. The findings reflect the results of the Mg– $x$ Al–3Sn samples with the rolling reduction of 40% in our previous research. This is because ETs exhibit a lower CRSS [25], while CTs can easily transformed into DTs during plastic deformation [26]. Furthermore, it has been reported that DRXed grains tend to originate from DTs [27] because DTs can serve as more efficient nucleation sites for DRXed grains

compared to ETs [28]. Al addition can increase the CRSS of twinning nucleation; therefore, the proportion of DTs decreases with the increasing Al content. Furthermore, with the increase in the rolling reduction to 60%, 3wt% added Al promotes the activation of DTs, while added Al inhibits the DTs. In other words, ATZ331-60% sample shows the highest frequency of 38° DTs, leading to the largest reduction of basal texture intensity.

### Macrotexture evolution

The pole figures of (002) and (101) planes are examined, as shown in Fig. 13, and the basal texture intensity of (002) plane is shown in Fig. 14. Results indicate that ATZ331 samples exhibit the lowest maximum intensity among these three samples regardless of the rolling reductions. As mentioned above, the frequency of substructure in the ATZ331 samples is higher than that in the Mg–3Sn and ATZ631 samples, as shown in Fig. 6, which can weaken the basal texture [29]. Consequently, ATZ331 samples exhibit the weakest basal texture. Moreover, when the rolling reduction ranges from 20 to 60%, the maximum basal texture intensity of all these three alloys first decreases and then increases, as shown in Fig. 14. For example, for the ATZ331 samples,





	Twin style	Misorientation angle	Rotation axis
Gray line	Grain boundary	2°~180°	-
Red line	{10-12} Extension Twin	86°	<11-20>
Green line	{10-11} Contraction Twin	56°	<11-20>
Blue line	{10-11}-{10-12} Double Twin	38°	<11-20>

**Figure 11** Misorientation angle maps of the samples with the rolling reduction of 60% **a, d** Mg–3Sn, **b, e** ATZ331 and **c, f** ATZ631 alloy.

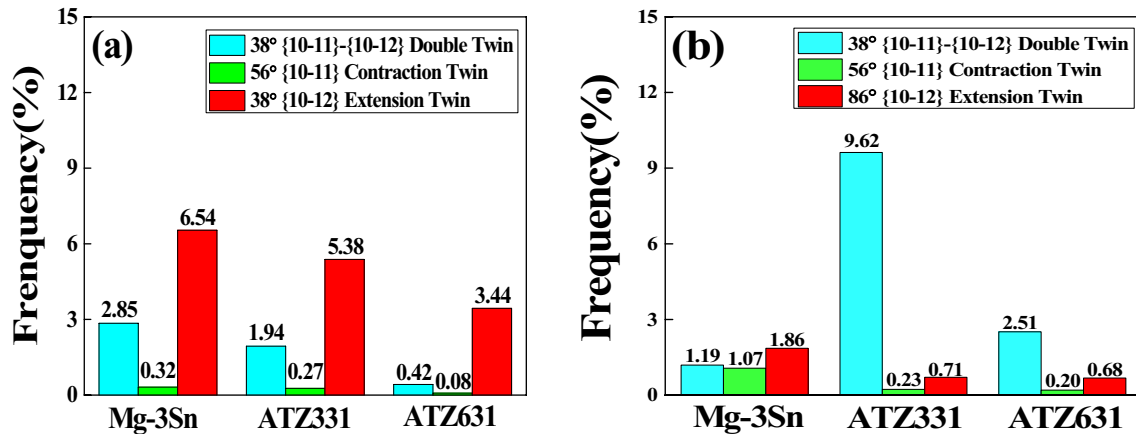


**Figure 12** The twin frequency of the HSRed Mg–xAl–3Sn samples with the rolling reduction of **a** 20% and **b** 60.

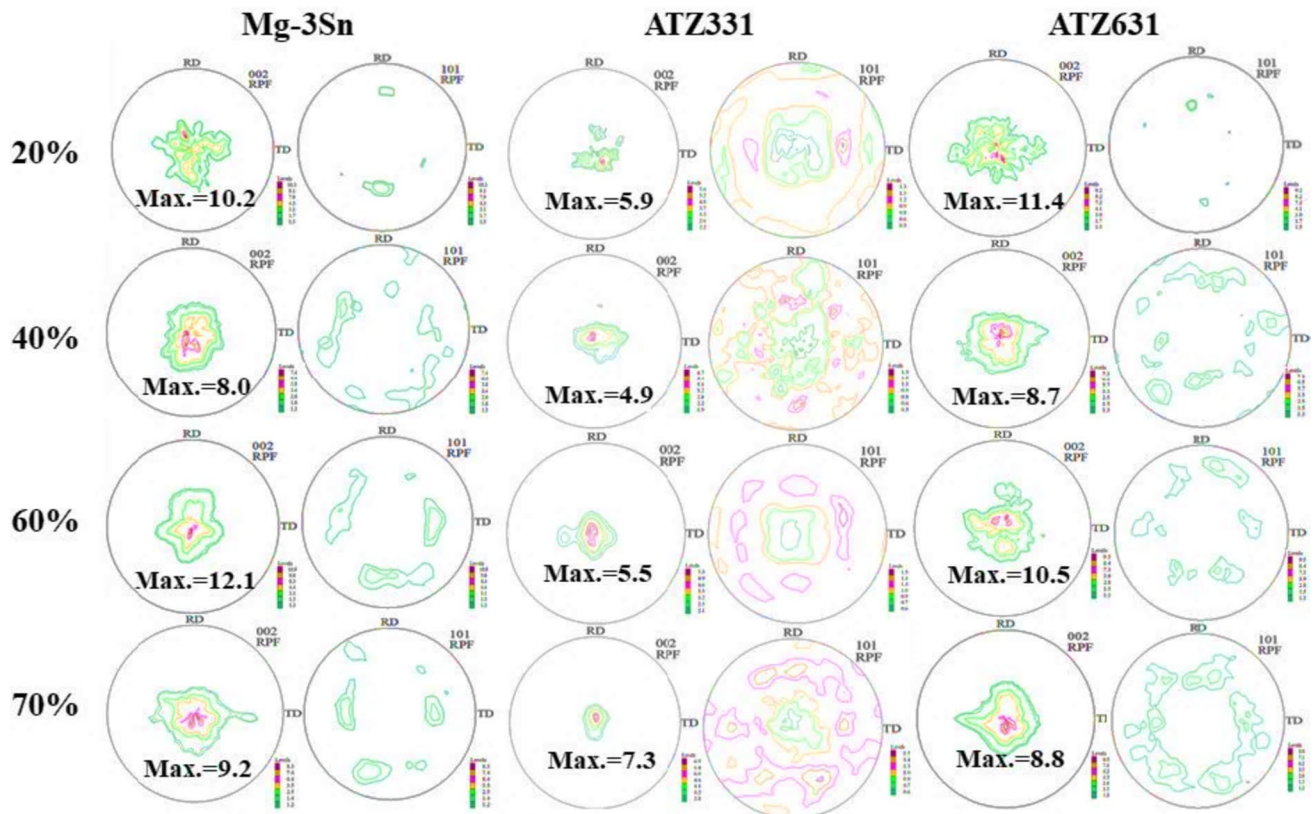


**Figure 13** Texture evolution of the Mg- $x$ Al-3Sn alloys with different rolling reductions.

the frequency of the substructure increases from 76 to 88% and then decreased to 79%, which, in turn, corresponded to variation in the maximum basal

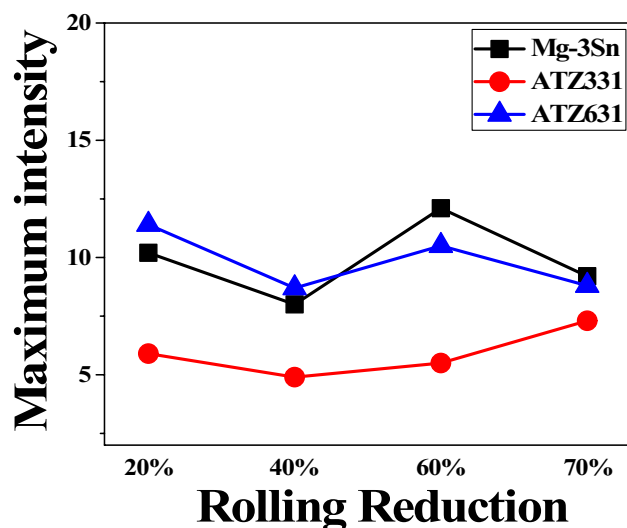


**Figure 14** The basal texture intensity of the Mg- $x$ Al-3Sn alloys with different rolling reductions.

texture intensity. However, when the rolling reduction increases further up to 70%, the basal texture of Mg-3Sn and ATZ631 samples weakens, presumably because the frequency of DRXed region increases with an increase in the rolling reduction (see Fig. 6). However, the basal texture of the ATZ331 sample is enhanced by lattice rotation of many more DRXed grains via dislocation slip during further deformation [6], exhibiting a typical rolling texture, as shown in Fig. 13.

## Conclusions

Mg- $x$ Al-3Sn ( $x = 0, 3, 6$ ) alloys with the rolling reductions of 20%, 40%, 60%, and 70% were successfully obtained in one pass by HSR at the rolling speed of 1100 m/min and the rolling temperature of 400 °C. This study contributes to our understanding of Al addition and rolling reduction on microstructural and texture evolution in Mg-3Sn alloys during HSR. The obtained conclusions are as follows:

- (1) During this process, the primary deformation mechanism is twinning, and the prominent nucleation mechanism is twinning-induced CDRX. First, numerous twins with high dislocation density are generated. Then, substructures and subgrains are formed as the potential nuclei for recrystallized grains within twins by the combined action of LAGBs and dislocations.
- (2) The main microstructure of the HSRed Mg–xAl–3Sn samples with various rolling reductions is substructure, and the orientation of substructure formed by twinning-induced DRX is decided by the initial twin type.
- (3) DRX behavior is the main factor influencing the basal texture. ATZ331 samples have the lowest maximum intensity irrespective of the rolling reductions. When the rolling reduction ranges from 20 to 60%, the maximum intensity of all these three alloys first decreases and then increases. However, with the further increase in the rolling reduction to 70%, the basal texture of Mg–3Sn and ATZ631 samples weakens, while that of ATZ331 sample strengthens.

## Acknowledgements

Not Applicable

## Author contributions

PD was involved in Investigation, Data curation, Writing—original draft, Methodology, and Formal analysis. WL contributed to Project administration and Funding acquisition. HX was involved in Data curation, Resources, and Data curation. LX contributed to Conceptualization, Methodology, Project administration, and Writing—review & editing. WX was involved in Validation and Supervision.

## Data availability

Data will be made available on request.

## Declarations

**Conflict of interest** The authors declare that they have no known competing financial interests or personal relationships that could have appeared to influence the work reported in this paper.

**Ethical approval** Not Applicable.

## References

- [1] Li X, Li Q (2020) Effect of pre-compression on microstructural evolution, mechanical property and strengthening mechanism of AZ31 alloy. *J Mater Sci* 55:11637–11649. <https://doi.org/10.1007/s10853-020-04724-1>
- [2] Chang G, Li W, Deng G, Liu Y (2023) Improvement of dynamic compression properties and strengthening mechanism of Mg–Y–Nd–Gd–Zr alloy by pre-twinning. *J Mater Sci* 58:8515–8534. <https://doi.org/10.1007/s10853-023-08521-4>
- [3] Pei D, Wang L, Yan T, Li X, Wang X (2022) Effect of Al addition and annealing on the microstructure evolution of Mg–3Sn Mg alloy subjected to high-speed rolling. *J Alloys Compd* 929:167224. <https://doi.org/10.1016/j.jallcom.2022.167224>
- [4] Su J, Sanjari M, Kabir ASH, Jung IH, Jonas JJ, Yue S, Utsunomiya H (2015) Characteristics of magnesium AZ31 alloys subjected to high speed rolling. *Mater Sci Eng A* 636:582–592. <https://doi.org/10.1016/j.msea.2015.03.083>
- [5] Kim SH, Lee JH, Lee CS, Yoon J, Park SH (2019) Dynamic deformation behavior and microstructural evolution during high-speed rolling of Mg alloy having non-basal texture. *J Mater Sci Technol* 35:473–482. <https://doi.org/10.1016/j.jmst.2018.10.010>
- [6] Lee JH, Lee JU, Kim SH, Song SW, Lee CS, Park SH (2018) Dynamic recrystallization and microstructural evolution of Mg alloy AZ31 through high-speed rolling. *J Mater Sci Technol* 34:1747–1755. <https://doi.org/10.1016/j.jmst.2018.03.002>
- [7] Wang X, Wang Y, Wang C, Xu S, Rong J, Yang Z, Wang J, Wang H (2020) A simultaneous improvement of both strength and ductility by Sn addition in as-extruded Mg–6Al–4Zn alloy. *J Mater Sci Technol* 49:117–125. <https://doi.org/10.1016/j.jmst.2019.04.048>
- [8] Zeng Y, Shi OL, Jiang B, Quan GF, Pan FS (2018) Improved formability with theoretical critical shear strength transforming in Mg alloys with Sn addition. *J Alloys Compd* 764:555–564. <https://doi.org/10.1016/j.jallcom.2018.06.055>

- [9] Wang H, Zhang N, Wang C, Jiang Q (2011) First-principles study of the generalized stacking fault energy in Mg-3Al-3Sn alloy. *Scr Mater* 65:723–726. <https://doi.org/10.1016/j.Scr.mat.2011.07.016>
- [10] Xie D, Pan H, Li M, Li J, Ren Y, Huang Q, Yang C, Ma L, Qin G (2020) Role of Al addition in modifying microstructure and mechanical properties of Mg-1.0wt% Ca based alloys. *Mater Charact* 169:110608. <https://doi.org/10.1016/j.matchar.2020.110608>
- [11] Tahreen N, Chen DL, Nouri M, Li DY (2015) Influence of aluminum content on twinning and texture development of cast Mg–Al–Zn alloy during compression. *J Alloys Compd* 623:15–23. <https://doi.org/10.1016/j.jallcom.2014.10.096>
- [12] Jin Z, Cheng X, Zha M, Rong J, Zhang H, Wang J, Wang C, Li Z, Wang H (2019) Effect of Mg<sub>17</sub>Al<sub>12</sub> second phase particles on twinning-induced recrystallization behavior in Mg–Al–Zn alloys during gradient hot rolling. *J Mater Sci Technol* 35:2017–2026. <https://doi.org/10.1016/j.jmst.2019.05.017>
- [13] Pei D, Wang L, Ge Z, Yuan Z, Hu X, Li X, Wang X (2023) Microstructure evolution and mechanical properties of Mg–3Al–3Sn–1Zn alloy during multi-pass high-speed rolling. *J Alloys Compd* 958:170406. <https://doi.org/10.1016/j.jallcom.2023.170406>
- [14] Harosh S, Miller L, Levi G, Bamberger M (2007) Microstructure and properties of Mg-5.6%Sn-4.4%Zn-2.1%Al alloy. *J Mater Sci* 42:9983–9989. <https://doi.org/10.1007/s10853-007-2059-y>
- [15] Zhu SQ, Yan HG, Chen JH, Wu YZ, Liu JZ, Tian J (2010) Effect of twinning and dynamic recrystallization on the high strain rate rolling process. *Scr Mater* 63:985–988. <https://doi.org/10.1016/j.Scr.mat.2010.07.029>
- [16] Ghazisaeidi M, Hector LG, Curtin WA (2014) Solute strengthening of twinning dislocations in Mg alloys. *Acta Mater* 80:278–287. <https://doi.org/10.1016/j.actamat.2014.07.045>
- [17] Tan JC, Tan MJ (2003) Dynamic continuous recrystallization characteristics in two stage deformation of Mg–3Al–1Zn alloy sheet. *Mater Sci Eng A* 339:124–132. [https://doi.org/10.1016/S0921-5093\(02\)00096-5](https://doi.org/10.1016/S0921-5093(02)00096-5)
- [18] Zhang J, Chen B, Liu C (2014) An investigation of dynamic recrystallization of ZK60–Er magnesium alloy. *Mater Sci Eng A* 612:253–266. <https://doi.org/10.1016/j.msea.2014.06.058>
- [19] Sanjari M, Farzadfar SA, Utsunomiya H, Sakai EE, Yue S (2012) High speed rolling of Mg–3Al–1Zn alloy: texture and microstructure analysis. *Mater Sci Technol* 28:928–933. <https://doi.org/10.1179/1743284712Y.0000000030>
- [20] Pan H, Qin G, Huang Y, Ren Y, Sha X, Han X, Liu Z, Li C, Wu X, Chen H, He C, Chai L, Wang Y, Nie J (2018) Development of low-alloyed and rare-earth-free magnesium alloys having ultra-high strength. *Acta Mater* 149:350–363. <https://doi.org/10.1016/j.actamat.2018.03.002>
- [21] Guan D, Rainforth WM, Ma L, Wynne B, Gao J (2017) Twin recrystallization mechanisms and exceptional contribution to texture evolution during annealing in a magnesium alloy. *Acta Mater* 126:132–144. <https://doi.org/10.1016/j.actamat.2016.12.058>
- [22] Guan D, Rainforth WM, Gao J, Sharp J, Wynne B, Ma L (2017) Individual effect of recrystallization nucleation sites on texture weakening in a magnesium alloy: part 1-DTs. *Acta Mater* 135:14–24. <https://doi.org/10.1016/j.actamat.2017.06.015>
- [23] Fan HD, Aubry S, Arsenlis A, Awady JA (2015) The role of twinning deformation on the hardening response of polycrystalline magnesium from discrete dislocation dynamics simulation. *Acta Mater* 92:126–139. <https://doi.org/10.1016/j.actamat.2015.03.039>
- [24] Al-Samman T, Molodov KD, Molodov DA, Gottstein G, Suwas S (2012) Softening and dynamic recrystallization in magnesium single crystals during c-axis compression. *Acta Mater* 60:537–545. <https://doi.org/10.1016/j.actamat.2011.10.013>
- [25] Jiang MG, Yan H, Chen RS (2015) Twinning, recrystallization and texture development during multi-directional impact forging in an AZ61 Mg alloy. *J Alloys Compd* 650:399–409. <https://doi.org/10.1016/j.jallcom.2015.07.281>
- [26] Niknejad S, Esmaili S, Zhou Y (2016) The role of double twinning on transgranular fracture in magnesium AZ61 in a localized stress field. *Acta Mater* 102:1–16. <https://doi.org/10.1016/j.actamat.2015.09.026>
- [27] Lee JH, Lee SW, Park SH (2019) Microstructural characteristics of magnesium alloy sheets subjected to high-speed rolling and their rolling temperature dependence. *J Mater Res Technol* 8:3167–3174. <https://doi.org/10.1016/j.jmrt.2018.11.020>
- [28] Levinson A, Mishra RK, Doherty RD, Kalidindi SR (2013) Influence of deformation twinning on static annealing of AZ31 Mg alloy. *Acta Mater* 61:5966–5978. <https://doi.org/10.1016/j.actamat.2013.06.037>
- [29] Nakata T, Mezaki T, Xu C, Oh-ishi K, Shimizu K, Hanaki S, Kamado S (2015) Improving tensile properties of dilute Mg-0.27Al-0.13Ca-0.21Mn (at.%) alloy by low temperature high speed extrusion. *J Alloys Compd* 648:428–437. <https://doi.org/10.1016/j.jallcom.2015.07.051>

**Publisher's Note** Springer Nature remains neutral with regard to jurisdictional claims in published maps and institutional affiliations.

Springer Nature or its licensor (e.g. a society or other partner) holds exclusive rights to this article under a publishing

agreement with the author(s) or other rightsholder(s); author self-archiving of the accepted manuscript version of this article is solely governed by the terms of such publishing agreement and applicable law.